ISPRS Journal of Photogrammetry and Remote Sensing 74 (2012) 20–33

Contents lists available at SciVerse ScienceDirect

ISPRS Journal of Photogrammetry and Remote Sensing

journal homepage: www.elsevier.com/locate/isprsjprs

Mapping tropical forests and rubber plantations in complex landscapes by integrating PALSAR and MODIS imagery

Jinwei Dong [a,*], Xiangming Xiao [a], Sage Sheldon [a], Chandrashekhar Biradar [a], Guishui Xie [b]

[a] Department of Botany and Microbiology, and Center for Spatial Analysis, University of Oklahoma, 101 David L. Boren Blvd., Norman, OK 73019, USA
[b] Rubber Research Institute, Chinese Academy of Tropical Agricultural Sciences, Baodaoxincun, Danzhou, Hainan 571737, China

ARTICLE INFO

Article history:
Received 31 October 2011
Received in revised form 15 July 2012
Accepted 23 July 2012
Available online 21 September 2012

Keywords:
PALSAR
MODIS
Evergreen forest
Deciduous forest
Rubber plantation
Hainan

ABSTRACT

Knowledge of the spatial distribution of forest types in tropical regions is important for implementation of Reducing Emissions from Deforestation and Forest Degradation (REDD), better understanding of the global carbon cycle, and optimal forest management. Frequent cloud cover in moist tropical regions poses challenges for using optical images to map and monitor forests. Recently, Japan Aerospace Exploration Agency (JAXA) released a 50 m orthorectified mosaic product from the Phased Array Type L-band Synthetic Aperture Radar (PALSAR) onboard the Advanced Land Observing Satellite (ALOS). PALSAR data provides information about the land surface without cloud interference. In this study we use the fine beam dual (FBD) polarization PALSAR 50 m mosaic imagery and a Neural Network (NN) method to produce a land cover map in Hainan Island, China. Subsequently, forest areas are classified into evergreen and deciduous forests and rubber plantations are mapped using vegetation and land surface water indices derived from 250 to 500 m resolution MODIS products. The PALSAR 50 m forest cover map, MODIS-based forest types and rubber plantation maps are fused to generate fractional maps of evergreen forest, deciduous forest and rubber plantation within 500 m or 250 m pixels. PALSAR data perform well for land cover classification (overall accuracy = 89% and Kappa Coefficient = 0.79) and forest identification (both the Producer's Accuracy and User's Accuracy are higher than 92%). The resulting land cover maps of forest, cropland, water and urban lands are consistent with the National Land Cover Dataset of China in 2005 (NLCD-2005). Validation from ground truth samples indicates that the resultant rubber plantation map is highly accurate (the overall accuracy = 85%). Overall, this study provides insight on the potential of integrating cloud-free 50 m PALSAR and temporal MODIS data on mapping forest types and rubber plantations in moist tropical regions.

1. Introduction

Tropical forests play an important role in the terrestrial carbon cycle and reduce the amount of greenhouse gases such as carbon dioxide (CO_2), carbon monoxide (CO) and nitrogen monoxide (NO) in the atmosphere (Lelieveld et al., 2008). Tropical forests also provide many ecosystem services that substantially affect human well-being (Foley et al., 2005; Pielke, 2005). Both human-induced deforestation (primarily to convert land to agricultural uses) and natural disturbance (e.g. fire, drought, wind blow-down) occur extensively in tropical regions (Bond-Lamberty et al., 2007; Kummer and Turner, 1994; Page et al., 2002; Sakaguchi et al., 2011). Plantations used for production of biofuels (e.g. oil palm) and industrial resources (e.g. rubber, *Hevea brasiliensis*) have expanded rapidly in tropical regions in the last 50 years (Fox and Vogler, 2005). This expansion has brought along a detrimental cascade of environmental effects including increasing threats to biodiversity and reduction in forest carbon stocks (Li et al., 2007; Ziegler et al., 2009). Accurate information on the area and spatial distribution of natural and planted forests in tropical areas is necessary for the implementation of Reducing Emissions from Deforestation and Forest Degradation (REDD) (Achard et al., 2007) and for modeling global carbon cycles (Dixon et al., 1994).

During the past few decades, optical remote sensing has been widely utilized for forest mapping (Asner et al., 2005; Collins et al., 2004; Thessler et al., 2008; Xiao et al., 2009, 2002). Previous studies have explored the potential for tropical forest mapping using imagery from the Advanced Very High Resolution Radiometer (AVHRR) (Achard and Estreguil, 1995; Achard et al., 2001), SPOT4-VEGETATION (Stibig et al., 2004; Stibig and Malingreau, 2003) and Moderate Resolution Imaging Spectroradiometer (MODIS) (Miettinen et al., 2012). Most of these studies employed

* Corresponding author. Tel.: +1 405 325 6091.
E-mail addresses: jinwei.dong@ou.edu (J. Dong), xiangming.xiao@ou.edu (X. Xiao), sage.sheldon@ou.edu (S. Sheldon), chandra.biradar@ou.edu (C. Biradar).

0924-2716/$ - see front matter © 2012 International Society for Photogrammetry and Remote Sensing, Inc. (ISPRS) Published by Elsevier B.V. All rights reserved.
http://dx.doi.org/10.1016/j.isprsjprs.2012.07.004

unsupervised classification due to the difficulty of ground truth sampling in tropical forest regions. Landsat Thematic Mapper (TM) images with 30 m spatial resolution and a 16-day revisit cycle are an important data source (Huang et al., 2009; Townshend and Justice, 1988); however, it is often difficult to obtain cloud-free Landsat images in tropical regions due to frequent cloud cover and moist climate (Asner, 2001). The images from the MODIS sensors have been used to map forest and detect deforestation at regional and global scales (Friedl et al., 2002; Giri et al., 2005; Morton et al., 2005; Tottrup et al., 2007; Xiao et al., 2009). Daily image acquisition by the MODIS sensors partly reduces cloud problems as compared to Landsat, providing valuable information to identify and map different forest types (Friedl et al., 2002; Xiao et al., 2009, 2002). However, its relatively coarse spatial resolution (250–1000 m) makes it difficult to accurately quantify and map forest areas at the regional scale due to mixture of land cover types within pixels. High spatial resolution remotely sensed imagery (e.g. SPOT-5, IKONOS, and aerial photographs), on the order of 1–50 m, are a very effective data source for local land use and land cover classification (Kabir et al., 2010; Perea et al., 2010; Su et al., 2010), but are not widely used in regional level monitoring due to the high cost of image acquisition and intensive computation resource requirements.

Images from synthetic aperture radar (SAR) offer an alternative data source for mapping tropical forests (Ardila et al., 2010; Simard et al., 2000). The radar illuminates vegetation types with microwave energy, recording return energy that is related to aboveground biomass and structure. Longer radar wavelength L-band SAR is better suited to the delineation of forest than other wavelengths because of its greater penetration through the canopy (Baghdadi et al., 2009). The Phased Array Type L-band Synthetic Aperture Radar (PALSAR) data is not subject to cloud interference, making it a more effective data source for forest mapping at the regional scale in moist tropical regions. PALSAR is onboard the Advanced Land Observing Satellite (ALOS) launched by the Japan Aerospace Exploration Agency (JAXA) in January of 2006, and it provides polarimetric radar images for most of the global land surface. PALSAR images have been used for many applications, including forest, crop, and ice mapping (Torbick et al., 2011; Xiao et al., 2010; Xie et al., 2010; Yang et al., 2010). The PALSAR team has developed two data products for the public: (1) the PALSAR 50 m Orthorectified Mosaic Product, and (2) the PALSAR 500 m Browse Mosaic Product. The publically released PALSAR 50 m mosaic product covers a large portion of Asia, and has recently been evaluated for regional forest monitoring potential in insular Southeast Asia (Longepe et al., 2011; Miettinen and Liew, 2011) with positive results. However, further evaluation of the potential of PALSAR 50 m mosaic product for mapping tropical forests in many regions is needed along with the development of new methodologies to challenges in those regions with complex landscapes and land use.

Hainan Island, the most representative tropical region in China, underwent dramatic changes in land use and land cover during the past few decades (Liu et al., 2010; Xu et al., 2002; Zhang et al., 2010). With the increasing demand for rubber products, rubber plantations continue to expand in Southern China (Qiu, 2009; Ziegler et al., 2009). It is necessary to develop an accurate and updated rubber distribution map for improving our understanding of land use change and carbon and water cycles (Li and Fox, 2011, 2012). Hainan Island is now thought to have the largest area of rubber plantation in China (Chen et al., 2010). There is an increasing need

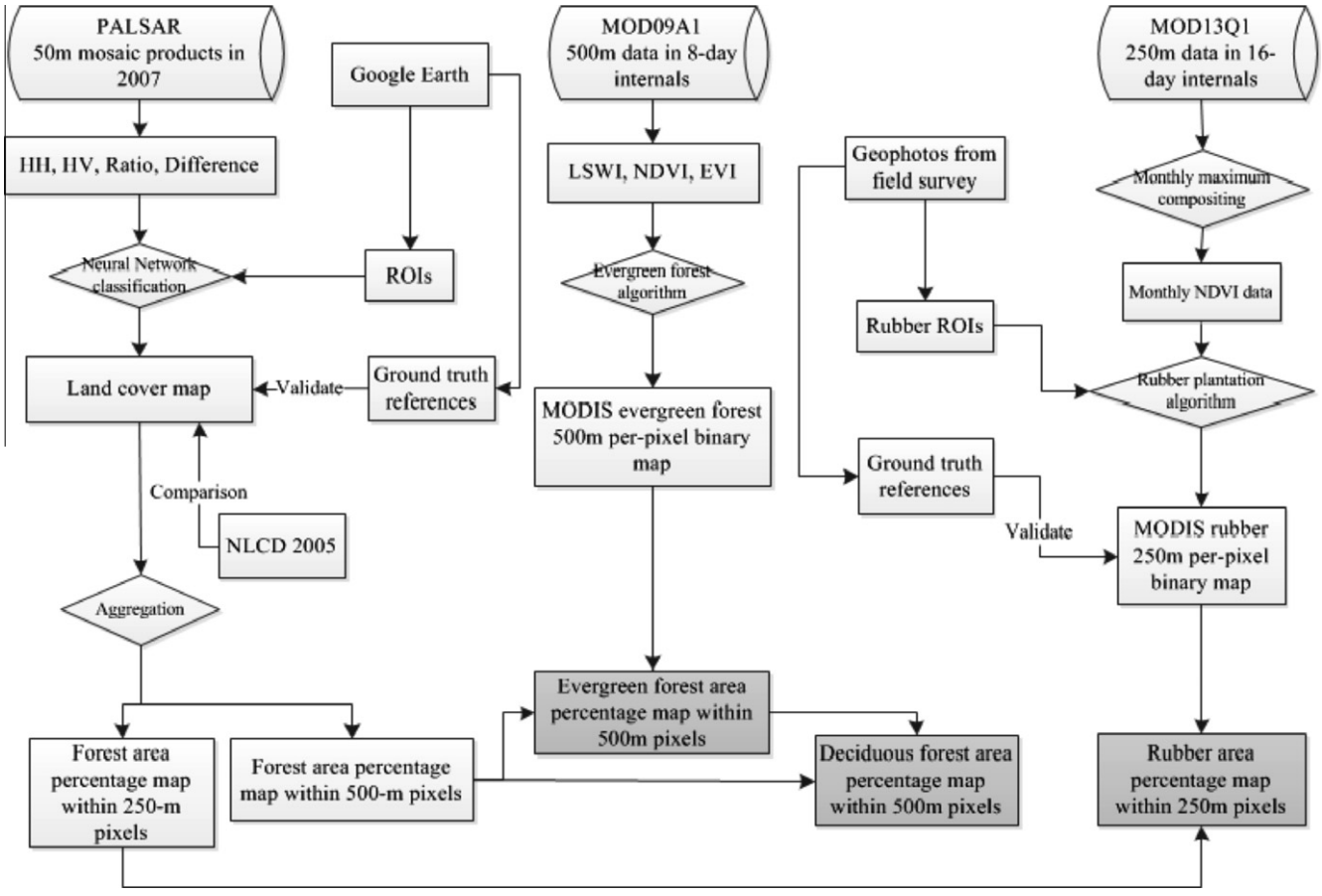

Fig. 1. The workflow of this study.

to obtain accurate information on the spatial distribution and areal extent of rubber plantations in Hainan Island.

The objective of this study was to quantify the extent and spatial distribution of evergreen and deciduous forests as well as rubber plantations on Hainan Island. PALSAR 50 m mosaic products and MODIS time series data (MOD09A1 and MOD13Q1) acquired in 2007 were used. This study was conducted through three components (Fig. 1): (a) creating a 50 m resolution land cover map with PALSAR mosaic data and aggregating the resultant map to produce forest percentage maps in 250 m and 500 m resolutions; (b) separating evergreen and deciduous forests as well as rubber plantations using a phenology-based approach with a time series of MODIS imagery; and (c) deriving area proportion distribution maps of evergreen, deciduous forests and rubber plantation by combining results from the previous two stages.

2. Materials and methods

2.1. A brief description of the study area

Hainan Island is located in southern China with a geographical area of 34,000 km^2, mostly located in a tropical area. The topography of the island is complex, characterized by hilly regions in the middle surrounded by lowlands in the coastal regions (Fig. 2). The Wuzhi Mountain is the highest mountain with an elevation of 1867 m above sea level. Climate on the island is characterized as a tropical monsoon climate. Annual mean temperature is approximately 23–25 °C and monthly temperature varies between ~16 °C in January to ~30 °C in May to July. Annual precipitation is approximately 1500 mm, and most of precipitation occurs between May and October.

There are a variety of vegetation types on the island. Historically, most of the island was covered by natural forests (Lin and Zhang, 2001); however, human exploitation has led to significant deforestation, and the natural forest area decreased from 1.2×10^4 km^2 in the 1950s to 0.42×10^4 km^2 in 1979 (Lin and Zhang, 2001). After 1994, extensive reforestation occurred on the island, and forest cover increased to 1.84×10^4 km^2 in 2004 (Hunan, 1999). Much of the newly planted areas were cash plantations which are included in the forest classes in the land cover classification developed in this study. The cropland area is approximately 0.73×10^4 km^2 and the agricultural intensity is high. At present, cash trees and crops, such as rubber, coconut, oil palm, and betel nut, are widely planted on the island. Human activities played an important role in these processes of deforestation, reforestation and land transformation. For example, several politico-economic activities such as the "rubber plantation campaign" in the 1950s, the "land reclamation campaign" in the 1960s, the "crop breeding campaign" in the 1970s, and the "open-door economic reform" in the 1980s (Cai, 1994; Christian and Narong, 2005) affected land use and land cover. Rubber plantations increased rapidly due to increasing rubber demand in recent decades, and a significant portion of natural tropical rainforest was converted into rubber plantations.

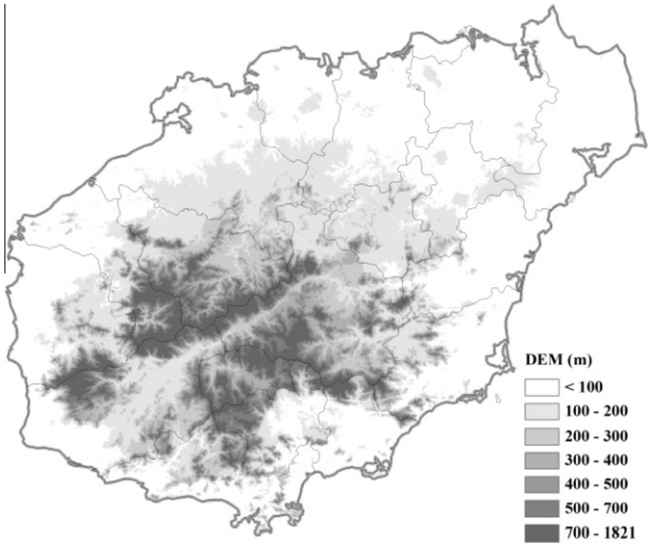

Fig. 2. Spatial distribution of terrain in Hainan Island, China. The DEM data is derived from the Shuttle Radar Topography Mission (SRTM) 90 m database.

2.2. Data

2.2.1. PALSAR data and pre-processing

The PALSAR 50 m Orthorectified Mosaic product is provided by JAXA and available at the ALOS Kyoto and Carbon Initiative official website (http://www.eorc.jaxa.jp/ALOS/en/kc_mosaic/kc_mosaic.htm). It is created from images of the ascending path. The original PALSAR images with an off-nadir angle of 34.3° were resampled into the 50 m by 50 m mosaic. The product is produced once a year and the dates of image acquisition vary between years. It has been geometrically rectified using 90 m digital elevation model (DEM) and geo-referenced into geographical latitude and longitude coordinates (Longepe et al., 2011).

In this study, we used HH and HV polarization data from the PALSAR 50 m mosaic product acquired with Fine Beam Dual (FBD) polarization observational mode in October 2007. We converted the Digital Number (DN) values (amplitude values) into normalized radar cross section in decibel (dB), based on the conversion formula from JAXA (Rosenqvist et al., 2007) and the parameters from the metadata file:

$$\sigma^0(\mathrm{dB}) = 10 \times \log_{10} DN^2 + CF \quad (1)$$

where σ^0 is the backscattering coefficient, DN is the digital number value of pixels in HH or HV, and CF is the absolute calibration factor.

We calculated two additional indicators using HH and HV data (dB data): (1) the ratio of HH and HV ($Ratio = HH/HV$) and (2) the difference between HH and HV ($Difference = HH–HV$). Both the Ratio and Difference images have been used in forest and forest change monitoring (Miettinen and Liew, 2011; Wu et al., 2011).

2.2.2. MODIS data and pre-processing

We used two MODIS products: (1) the 500 m MODIS land surface reflectance product (MOD09A1), which provides data in spectral ranges that most benefit the study of land surfaces and vegetation in an 8-day composite with quality screening; and (2) the 250 m vegetation indices product (MOD13Q1), which is designed to provide consistent spatial and temporal comparisons of vegetation conditions in 16-day intervals. Detailed information about these products is available on the site (http://lpdaac.usgs.gov/products/) maintained by the NASA Land Processes Distributed Active Archive Center (LP DAAC).

Three vegetation indexes, the Normalized Differential Vegetation Index (NDVI) (Tucker, 1979), the Enhanced Vegetation Index (EVI) (Huete et al., 2002, 1997), and the Land Surface Water Index (LSWI) (Xiao et al., 2004, 2005), were calculated from MOD09A1 data with the following formulas:

$$\mathrm{NDVI} = \frac{\rho_{NIR1} - \rho_{red}}{\rho_{NIR1} + \rho_{red}} \quad (2)$$

$$\mathrm{EVI} = 2.5 \times \frac{\rho_{NIR1} - \rho_{red}}{\rho_{NIR1} + 6 \times \rho_{red} - 7.5 \times \rho_{blue} + 1} \quad (3)$$

$$\mathrm{LSWI} = \frac{\rho_{NIR1} - \rho_{SWIR1}}{\rho_{NIR1} + \rho_{SWIR1}} \quad (4)$$

where ρ_{blue}, ρ_{red}, ρ_{NIR1}, and ρ_{SWIR1} are the reflectance values from the blue (459–479 nm), red (620–670 nm), NIR1 (841–875 nm) and SWIR1 (1628–1652 nm) bands, respectively. In this study we used 500 m NDVI, LSWI and EVI data in 8-day internals and 250 m NDVI data in 16-day internals.

2.3. Land cover map based on analysis of PALSAR 50 m mosaic data

Google Earth provides geometrically rectified images with a high horizontal accuracy and resolution (Potere, 2008), and has been utilized in several recent land cover classification studies (Cohen et al., 2010; Huang et al., 2010; Potere, 2008). In this study, we used Google Earth images over Hainan Island to collect a training dataset for land cover classification, and most of the images in Google Earth were acquired during 2006–2010, consistent with the time of PALSAR data (2007). From these images we selected 52 regions of interest (ROI) for forest, 54 for cropland, 12 for water, and 14 for urban land. The sizes of urban land and water ROIs were relatively large, as both water and urban land are distributed in large sizes and easy to extract. The ROI pixel numbers for four land covers were abundant.

The feed-forward Neural Network (NN) algorithm with one hidden layer (Richards and Jia, 2006) and PALSAR 50 m data (HH, HV, Ratio and Difference images) were used to map four land-cover types (forest, water, urban and cropland) of Hainan Island. A number of parameter compositions were tried and evaluated, and finally we verified and reported the parameters as following: the activation method was set as *Logistic*, with parameters viz.: *training threshold contribution* at 0.9, which determines the internal weights and affects the activation level of the nodes; *training rate* at 0.2, which decides the magnitude of the adjustment of the weights; *training momentum* at 0.9; *training RMS exit criteria* at 0.1; and *training iterations number* at 2500. Training data sets were essential for the NN classifier, as every sample was taken into consideration in the training (Kavzoglu, 2009). We applied the ROIs mentioned above to map land cover on the island.

Finally, the resultant 50 m PALSAR-based forest map provides more precise information for forest canopy cover than that from MODIS data (Fig. 6a). The PALSAR 50 m spatial resolution map was aggregated to calculate the percent forest canopy cover (%) within each MODIS pixel from MOD13Q1 (250 m) and MOD09A1 (500 m) products. These fractional cover maps of forest were later used together with the per-pixel binary maps of forests from MODIS to estimate the spatial distribution and areas of evergreen and deciduous forests.

2.4. Separating evergreen and deciduous forest with MOD09A1 data

Time series LSWI data from MODIS imagery was used for mapping evergreen forest based on its temporal profile characteristics (Xiao et al., 2009). The resultant outputs were tested against other existing global forest maps, such as the standard MODIS Land Cover data product (MOD12Q1) (Friedl et al., 2002), FAO FRA 2000, and GLC2000 (Bartholome and Belward, 2005). A MODIS pixel is assigned to evergreen forest if it has LSWI values larger than 0 in all good-quality observations throughout a year (Xiao et al., 2009); deciduous forests do not have all LSWI values above 0 for the entire year.

The resultant evergreen forest map from MOD09A1 imagery (Fig. 6c) was overlaid with the fractional map of forests from PALSAR imagery, and the total area of evergreen forest was calculated by summing the fractions of PALSAR-based forests within those MODIS-based evergreen forest pixels. We then considered the remaining forest area of the PALSAR-based forest map as deciduous forests.

2.5. Mapping rubber plantations using phenology from MOD13Q1 data

When rubber was introduced from British Malaya in the 20th century, Hainan Island was not a suitable environment for its cultivation. Subsequent improvement in rubber germplasm allowed it to adapt to the frequent typhoons and low winter temperatures of Hainan Island. Rubber plants on the island remain sensitive to temperature change, and have different phenological characteristics from natural forest and other cash forests such as *lichee* and *longan* (Chen et al., 2010). Rubber plantations have two distinct seasons in a year: a growing season and a non-growing season. In the growing season, rubber plantations have high NDVI values, similar to other evergreen forests. However, low temperatures in the winter ($\sim$10 °C) force rubber plants to defoliate, resulting in a canopy coverage of 20% (or less) and a low NDVI value (Chen et al., 2010).

We extracted the time series vegetation indices (NDVI, EVI and LSWI) from (1) one typical rubber site (Danzhou), which is the long-term study site of the Rubber Research Institute, Chinese Academy of Tropical Agricultural Sciences; (2) one evergreen forest site in southwestern Hainan Island; and (3) one paddy rice site in the Luodaixiang Town of Dongfang City (Fig. 3). The NDVI values of rubber plantation decreases substantially in the senescence period due to cold and rubber tapping, which starts from late October and ends in March of next year; and the lowest NDVI values appear in January, February and March. In the growing season, NDVI increases rapidly from the end of March to October (Fig. 3a). The temporal profiles of EVI and LSWI for rubber, paddy rice cropland and evergreen forests are different as well, but not as significant as NDVI (Fig. 3b and c). Therefore, we applied 250 m MOD13Q1 NDVI products to identify and delineate phenology of rubber plantation. In this study we only identify and map mature rubber plantation, as young rubber is easily confused with bare soil or crops, especially when rubber seedlings are intercropped with other crops.

The workflow for mapping rubber plantation is depicted in Fig. 1. Rubber plantation was identified with the following decision rule:

$$if\,(0.5 < \mathrm{NDVI}_{(Jan,Feb,Mar)} < 0.7 \cap 0.73 < \mathrm{NDVI}_{(May,Jun,Jul)} < 0.85), rubber = 1;\ else, rubber = 0$$

where $\mathrm{NDVI}_{(Jan,\ Feb,\ Mar)}$ and $\mathrm{NDVI}_{(May,\ Jun,\ Jul)}$ are the mean NDVI in January, February and March and the mean NDVI in May, June and July, respectively. The monthly NDVIs were calculated with the Maximum Value Composition (MVC) method from the 16-day composites in a month (most months have two 16-day composite data, but there is only one 16-day composite in November). The selection of the thresholds was basically based on a statistical analysis of 287 rubber plantation samples. For example, the $\mathrm{NDVI}_{(May,Jun,Jul)}$ of rubber samples had a mean value of 0.79 and a standard deviation of 0.06, we set the thresholds as the mean value minus and plus the standard deviation value; we further checked the data distribution and tested the thresholds, and finally verified 0.73 and 0.85 as the thresholds of $\mathrm{NDVI}_{(May,Jun,Jul)}$.

2.6. Accuracy assessment and comparison to other land cover datasets

We used both ground survey and Google Earth to evaluate the accuracy of the land cover maps produced in this study. Firstly, we linked the PALSAR-based land cover map with Google Earth and randomly selected 40 polygons (31,284 pixels) as ground reference from the Google Earth images for accuracy assessment. In order to assess the accuracy of the rubber plantation identification, we conducted a field survey in August of 2011 with a GPS digital camera as the main information capture tool. 87 georeferenced field photos were acquired in the plots where rubber plantation

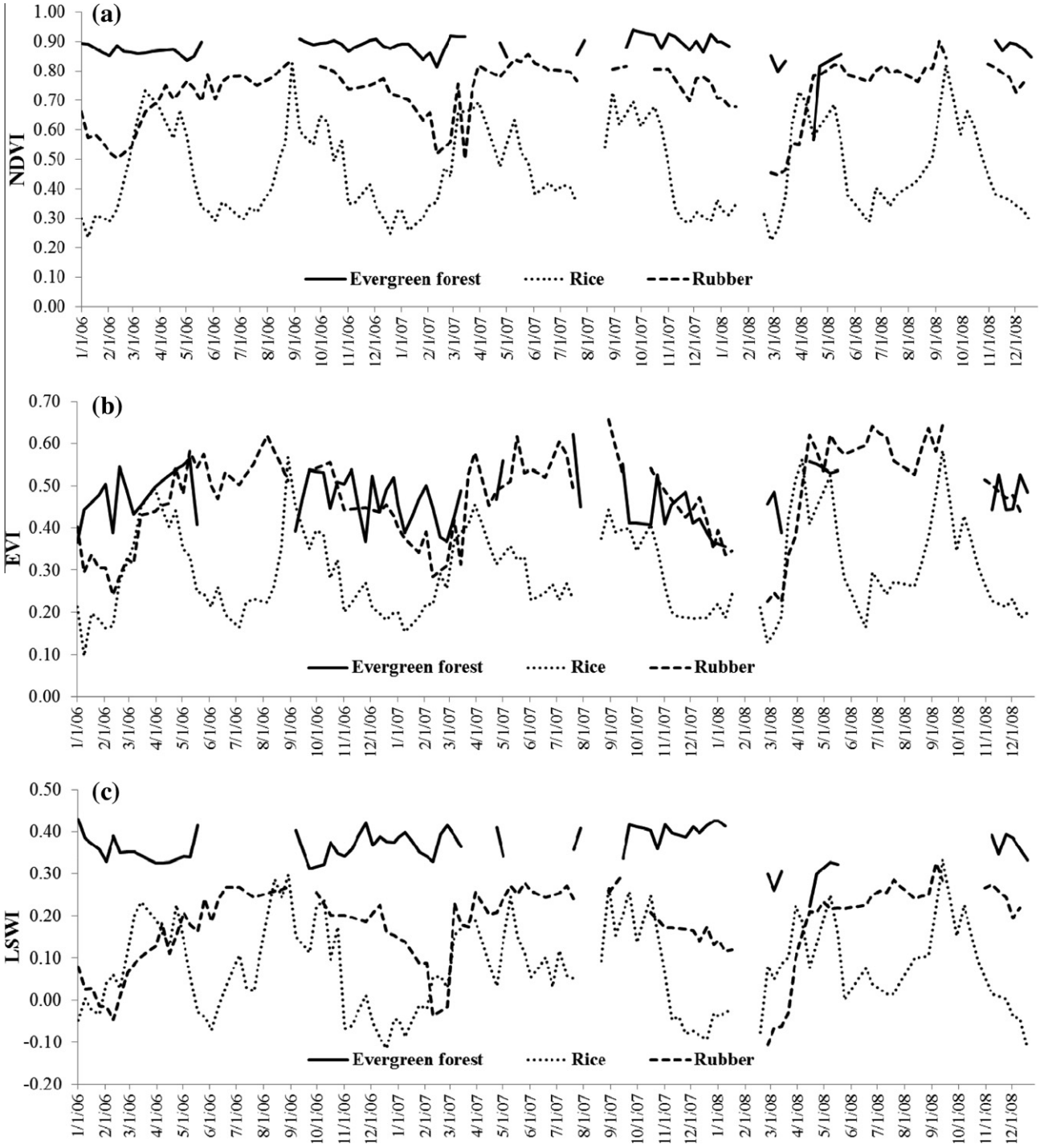

Fig. 3. Comparison between the temporal profiles of (a) NDVI, (b) EVI, and (c) LSWI for typical vegetation types (January 2006 to December 2008). The samples include (a) a rubber sample in Danzhou station (19.516 N, 109.47 E), which is a typical observational site of Rubber Research Institute, Chinese Academy of Tropical Agricultural Sciences; (b) an evergreen forest sample (18.718 N, 108.966 E) in southwestern Hainan Island; and (c) a paddy rice cropland sample (19.058 N, 108.676 E) in the Luodaixiang Town of Dongfang City, Hainan. There are some gaps in the curves as the values with low quality (e.g. intensive cloud coverage or shadow) were removed.

areas were larger than 500 m × 500 m. This data was also uploaded into an online system named the "Global Geo-Referenced Field Photo Library" (http://www.eomf.ou.edu/photos/). Subsequently, these plantation areas were outlined in Google Earth and used as ground truth polygons for evaluating the accuracy of the identification of rubber plantations.

We also compared the PALSAR-based land cover map with the Landsat-based National Land Cover Dataset (NLCD). The Chinese Academy of Sciences has supported the development of NLCD in China and developed a methodology based on visual interpretation and digitalization of Landsat imagery (Liu and Deng, 2010; Liu et al., 2010). The NLCD vector dataset has a scale of 1:100,000 (Liu et al., 2005). Four periods (the late 1980s, the mid-1990s, 2000, and 2005) of NLCD datasets have been completed, and they are comprehensive spatial datasets about land cover change at the national scale. In this study, we used the NLCD 2005 for comparison with the PALSAR-based land cover map.

3. Results

3.1. Landcover map of forest, cropland, urban and water from PALSAR in 2007

The signatures of four land cover types were explored in the HH, HV, Ratio image and Difference image based on the ROIs from Google Earth. The separability of these four land cover types was high (Fig. 4). Water has the lowest HH and HV values but higher Ratio values than the other three land cover types and is thus easily identified. Cropland has lower HV and HH values but higher Difference values than that of forest. Higher HV values were observed for the forests due to their large crown canopy which depolarizes incident radiation. Urban land has higher HH and Difference values than forest but lower Ratio values. However, urban land overlaps with forest to a large degree in all the four indicators due to complex reflectance environments in urban area, building orientations, corner reflectance, and large forest patches in urban areas.

The map produced with NN method is shown in Fig. 5a. The areas of the four land cover types are 2.07×10^4 km^2 forest; 1.06×10^4 km^2 cropland; 0.17×10^4 km^2 urban land; and 0.08×10^4 km^2 water body, respectively. The forests are mainly concentrated in higher elevations of the central hilly area. The cropland is distributed in a mosaic pattern in the lower elevations surrounded by forests. This indicates that topography (Fig. 2) plays a role in the spatial pattern of forests and cropland on the island. The two large cities, Haikou and Sanya, account for the majority of the urban land area. The PALSAR-based false color composite map clearly illustrates land cover separability (Fig. 5c).

The overall accuracy of the land cover map was 89% with Kappa Coefficient of 0.79 (Table 1). Both the Producer's Accuracy and the User's Accuracy of forest and water were more than 92% (Table 1). Cropland also had a high Producer's Accuracy (86%); however, the User's Accuracy of cropland was only 62%. The low User's Accuracy shows that cropland area was underestimated in some places, as different kinds of crops (e.g. fallowed cropland or different stages of crops) have various polarization signatures. Urban land had a Producer's Accuracy of 56% while its User's Accuracy was 74%, as some trees in cities affected the pixels of urban land. In general, the classification results had reasonably good accuracy for the four land cover types, especially forests.

A comparison between the PALSAR-based land cover map in 2007 (PALSAR 2007) and the NLCD 2005 map was conducted and a confusion matrix was generated to evaluate the consistency of the two land-cover classification results. Fig. 5a shows the spatial distribution of the PALSAR-based map, which is consistent with the NLCD 2005 dataset (Fig. 5b). Forests have a relatively high agreement; PALSAR-based forest area is 2.07×10^4 km^2

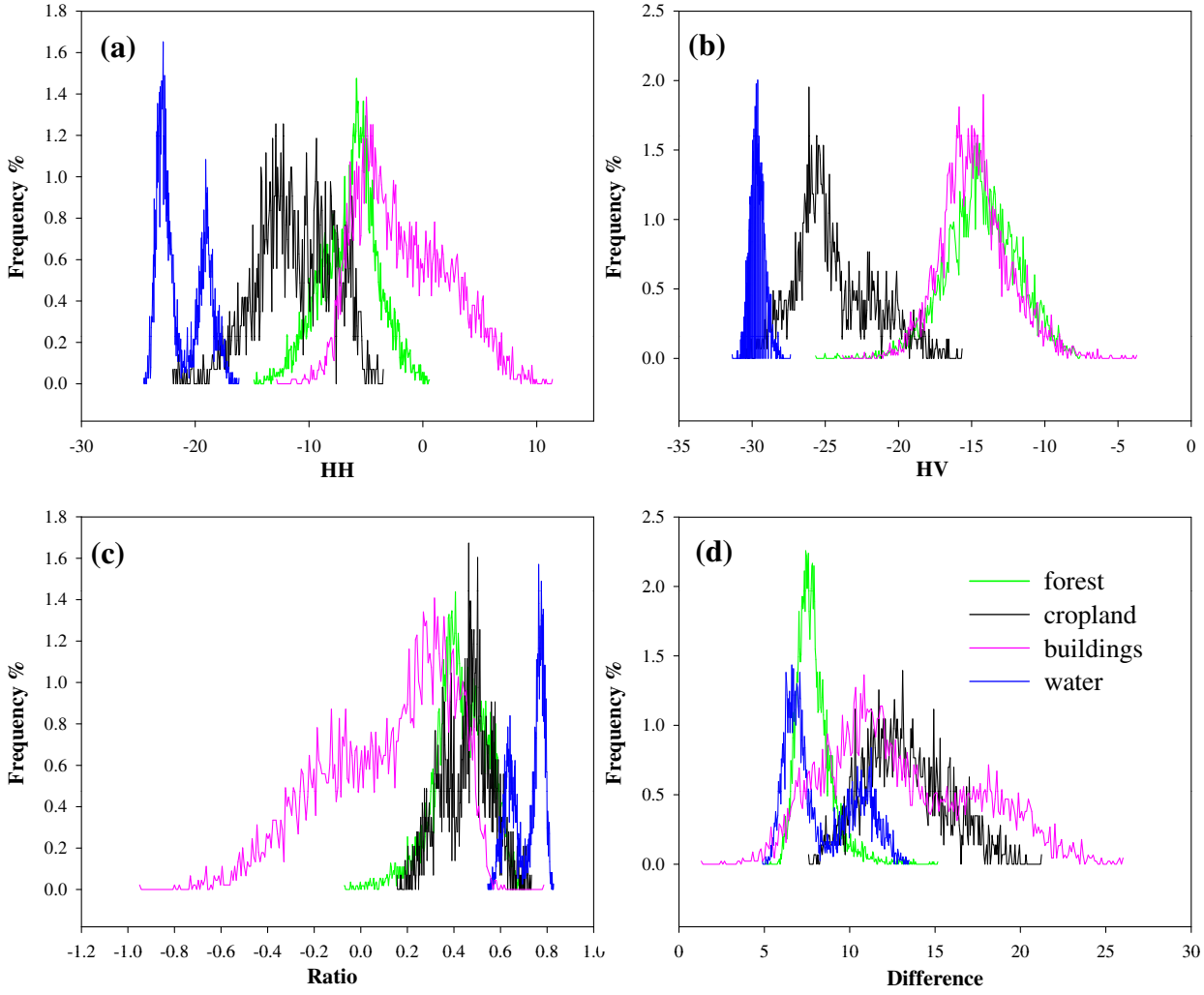

Fig. 4. The histogram of the four land cover types in (a) PALSAR HH polarization, (b) PALSAR HV polarization, (c) PALSAR HH/HV ratio image, and (d) PALSAR HH–HV difference image for all the pixels within the Region of Interest (ROIs) in Hainan Island, China.

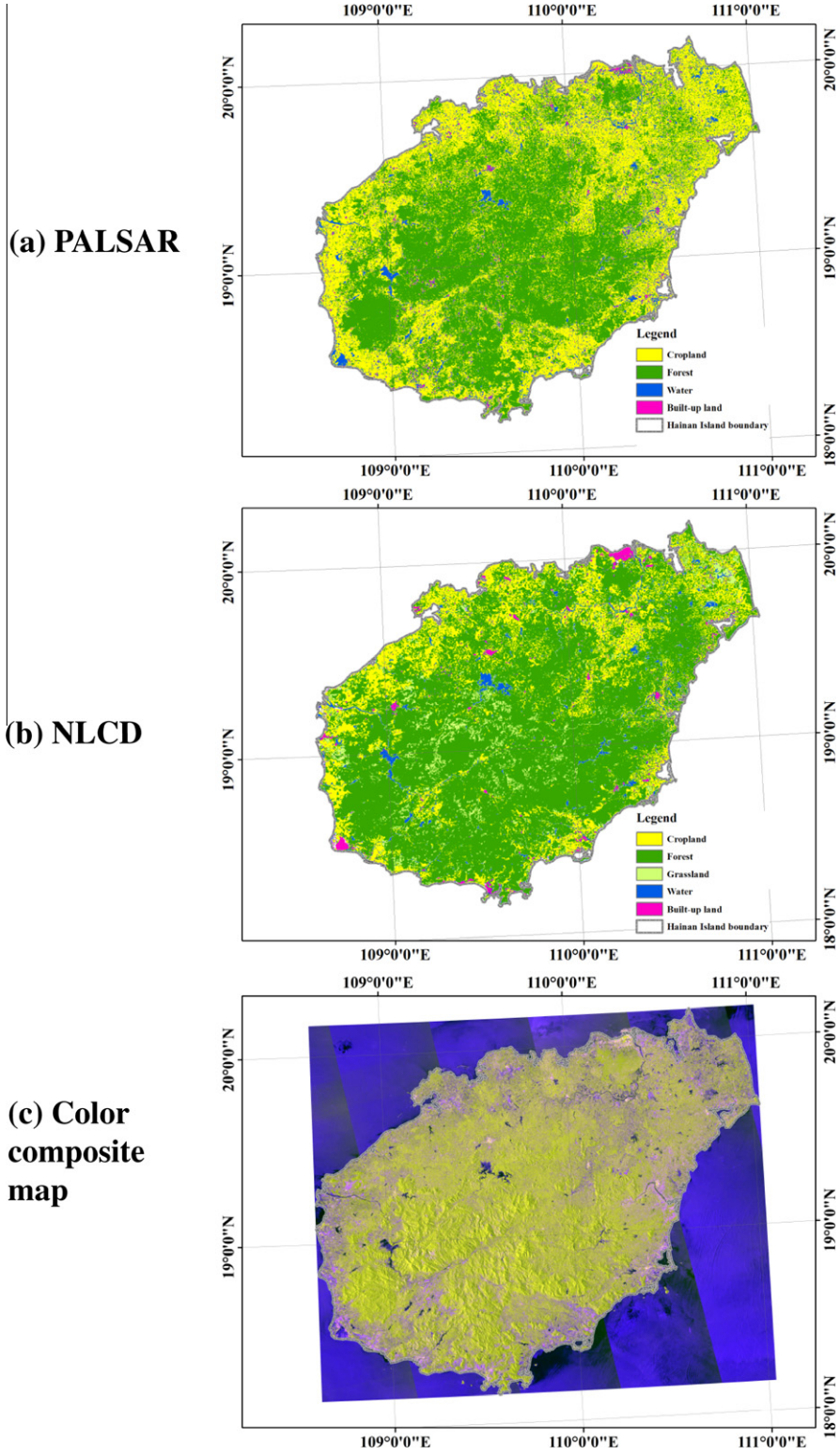

Fig. 5. A comparison between (a) PALSAR-based land cover map in 2007, (b) NLCD land cover map in 2005, and (c) PALSAR-based color composite map in 2007 (R/G/B = polarizations HH/HV/HH–HV Difference) in Hainan Island, China.

while the forest in NLCD is 2.17×10^4 km^2. The overlapped forest area between these two datasets is 1.63×10^4 km^2 (Table 2), which accounts for ~79% of forest in the PALSAR 2007 map and ~75% of forest in the NLCD 2005 dataset. The discrepancy between these two datasets could be attributed partly to the land use change from 2005 to 2007, and partly because the classification systems differ slightly. The estimates of cropland area from these two land-cover classification schemes differ somewhat (Table 2). It is possible that cropland in the NLCD 2005 dataset included different cropland types, such as fallowed cropland, and the classified cropland from PALSAR might have included some tall-grass grassland.

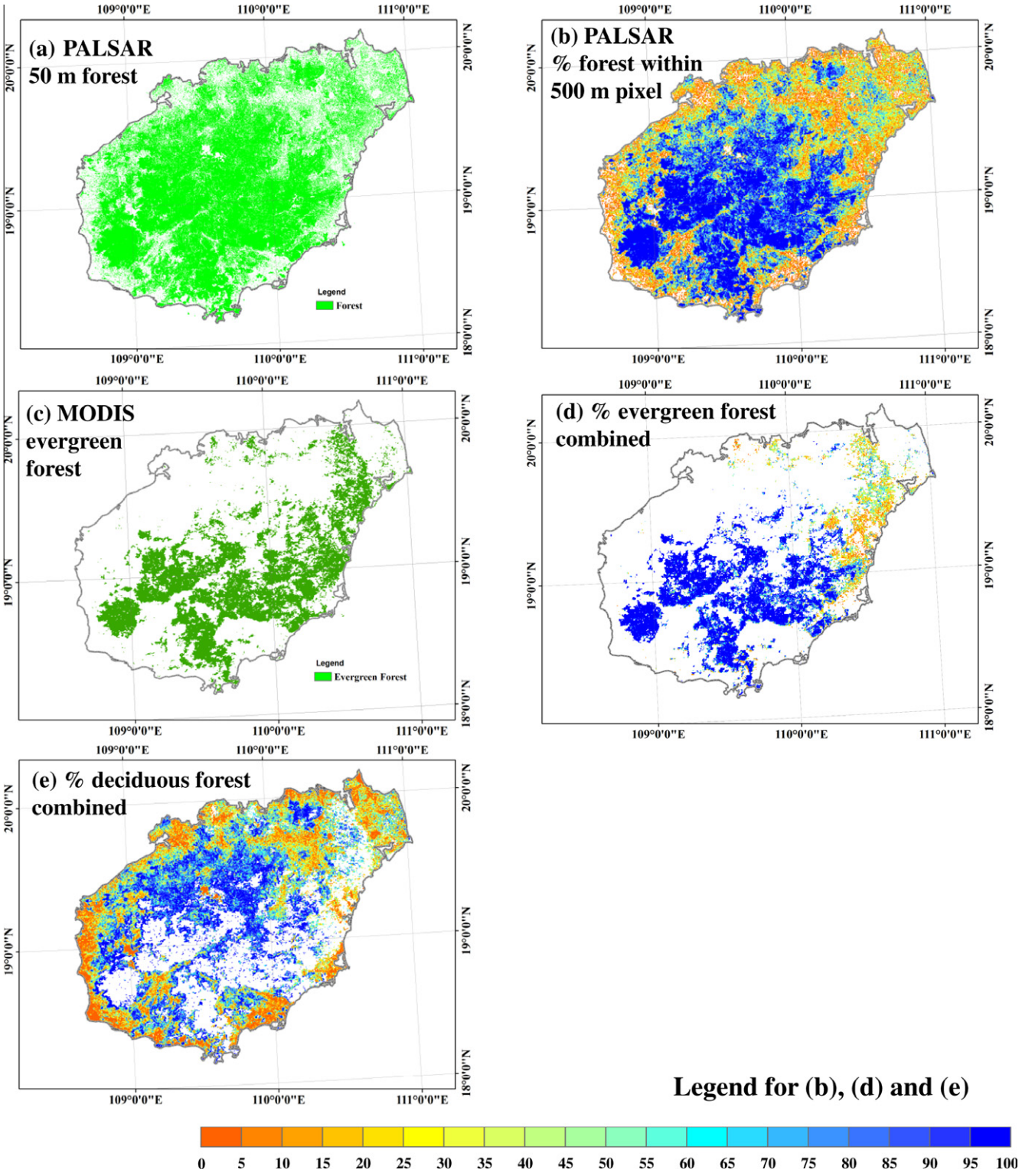

Fig. 6. (a) 50 m PALSAR-based per-pixel binary forest map; (b) 500 m forest area percentage map aggregated from the 50 m PALSAR-based forest map; (c) 500 m per-pixel binary map of evergreen forest based on MODIS LSWI analysis; (d) area percentage map of evergreen forest by overlaying per-pixel binary evergreen forest map *c* and 500 m forest area percentage map *b*; (e) area percentage map of deciduous forest by subtracting evergreen forest area percentage map *d* from 500 m forest area percentage map *b*.

3.2. The area and spatial distribution of evergreen and deciduous forests

The spatial distribution of forest area percentage within 500 m pixels is shown in Fig. 6b. The loss of forest area during the aggregation from 50 m spatial resolution (Fig. 6a) to 500 m and 250 m spatial resolutions was negligible. The 500 m pixels including forests covered 94% of the whole island area.

The spatial distribution of evergreen forest area percentage is shown in Fig. 6d. The area of evergreen forest was estimated to be approximately 0.75×10^4 km^2. Those evergreen forest pixels with high forest area percentage were concentrated in the middle

Table 1
A comparison between PALSAR land cover map and ground truth samples.

		Ground truth samples (unit: pixels)				PALSAR Total (pixel)	User acc. (%)
		Water	Forest	Cropland	Urban land		
PALSAR land cover classification	Water	5074	6	193	0	5273	96.23
	Forest	0	18,839	7	1564	20,410	92.30
	Cropland	113	193	1245	468	2019	61.66
	Urban land	0	943	3	2636	3582	73.59
Total ground truth samples (pixel)		5187	19,981	1448	4668	31,284	
Prod. acc. (%)		97.82	94.28	85.98	56.47		

Table 2
A comparison between PALSAR land cover map in 2007 and NLCD 2005 dataset.

		NLCD 2005 (km^2)					PALSAR total (km^2)
		Forest	Cropland	Water	Urban land	Others	
PALSAR 2007	Forest	16,268	3215	220	257	744	20,704
	Cropland	4382	5025	397	346	467	10,616
	Water	138	177	341	42	117	815
	Urban land	924	475	27	166	61	1654
NLCD total (km^2)		21,712	8892	984	811	1389	33,789

and southern regions with hilly topography, whereas the deciduous forests were mainly distributed in the northern parts of the island (Fig. 6e).

Fig. 7 shows the frequency distributions for forest percentage within 500 m and 250 m pixels for the evergreen forest pixels, deciduous forest pixels and rubber plantation pixels, and the region as a whole. Most of the evergreen forest pixels have high forest percentages; 49% of evergreen forest pixels have forest percentages ranging from 95% to 100%. In other words, 49% of MODIS-based evergreen forest pixels were almost pure evergreen forest. In addition, 70% of MODIS evergreen forest pixels have forest area percentages greater than 65%, which revealed that evergreen forest distribution was concentrated to a great extent. However, deciduous forest showed different characteristics from evergreen forest in that its distribution was more dispersed than that of evergreen forest. For example, 47% of 500 m deciduous forest pixels have forest area percentages larger than 60%, 53% of 500 m pixels have forest area percentages larger than 50%, and the 500 m pixels with forest area proportion less than 5% accounts for 10%.

3.3. The area and spatial distribution of rubber plantation in 2007

The spatial distribution of rubber plantations from analysis of MOD13Q1 (250 m) data in 2007 is shown in Fig. 8b. According to the ground sampling based accuracy assessment the mapping accuracy was high. The overall accuracy for rubber plantations was 85% with kappa of 0.83.

The NDVI-based rubber plantation map has 1.04×10^5 pixels of rubber plantations; it was overlaid with the PALSAR-based 250 m forest area percentage map in 2007 (Fig. 8a); and the resultant map is assumed to be the map of rubber plantation in 2007 (Fig. 8c). Approximately 43% of rubber plantation pixels (from MOD13Q1, 250 m resolution) have a rubber plantation area percentage of more than 95%, and 85% of rubber plantation pixels have rubber plantation area percentages larger than 50% (Fig. 7d). The total area of rubber plantations was calculated by summing forest area percentage over those rubber plantation pixels from the MOD13Q1 map (Fig. 8c), and it is estimated that there was a total of 5149 km^2 of rubber plantations on Hainan Island in 2007, which is about 7% larger than the area estimate (4800 km^2 in 2010) from the official statistical report (The Yearbook of Hainan Province in 2011).

4. Discussion

This study evaluated the application potential of PALSAR 50 m mosaic and MODIS data for delineation and mapping of forests in the tropical zone. The results were evaluated with ground truth data and compared to the Landsat-based NLCD 2005 map generated through visual interpretation. Our study revealed the advantages of PALSAR mosaic product as compared to Landsat images. The PALSAR-based forest area estimate (2.07×10^4 km^2) is closer to the land survey result (2.02×10^4 km^2) from the China Land Resource Bureau[1] than the Landsat-based NLCD-2005 data (2.17×10^4 km^2). In addition to the potential land cover changes that have taken place 2005–2007, these differences may be largely due to methodological differences and image data. Note that the NLCD-2005 land cover map was generated by visual interpretation based on color composition maps; forest and some crops could have similar optical (color) characteristics and are difficult to separate them in human-aid interpretation on a false color composite map. With comparison in some selected regions by zooming in the map, we found that the PALSAR 2007 dataset has a higher accuracy than the NLCD-2005 dataset. The maximum ability for human vision to distinguish land cover from Landsat images is about 3 pixels (about 100 m). Therefore, when compared to automated digital image classification, the visual interpretation method omits some information sometimes. The PALSAR 2007 forest map shows more spatial heterogeneity and has more specific details in the land parcels.

Before PALSAR, single HH polarization data from JERS-1 was widely used for forest mapping (e.g. clear-cut or biomass intensity) (Luckman et al., 1998; Simard et al., 2002). However, this single polarization-based algorithm has some shortcomings in forest delineation (Santoro et al., 2010). Multiple frequency, multiple polarization and time series of SAR data improves classification accuracy evidently (Ranson and Sun, 1994; Townsend, 2002). Sev-

[1] According to 'Outline of comprehensive land use planning of Hainan province (2006–2020)' by Yansui Liu et al. (2008).

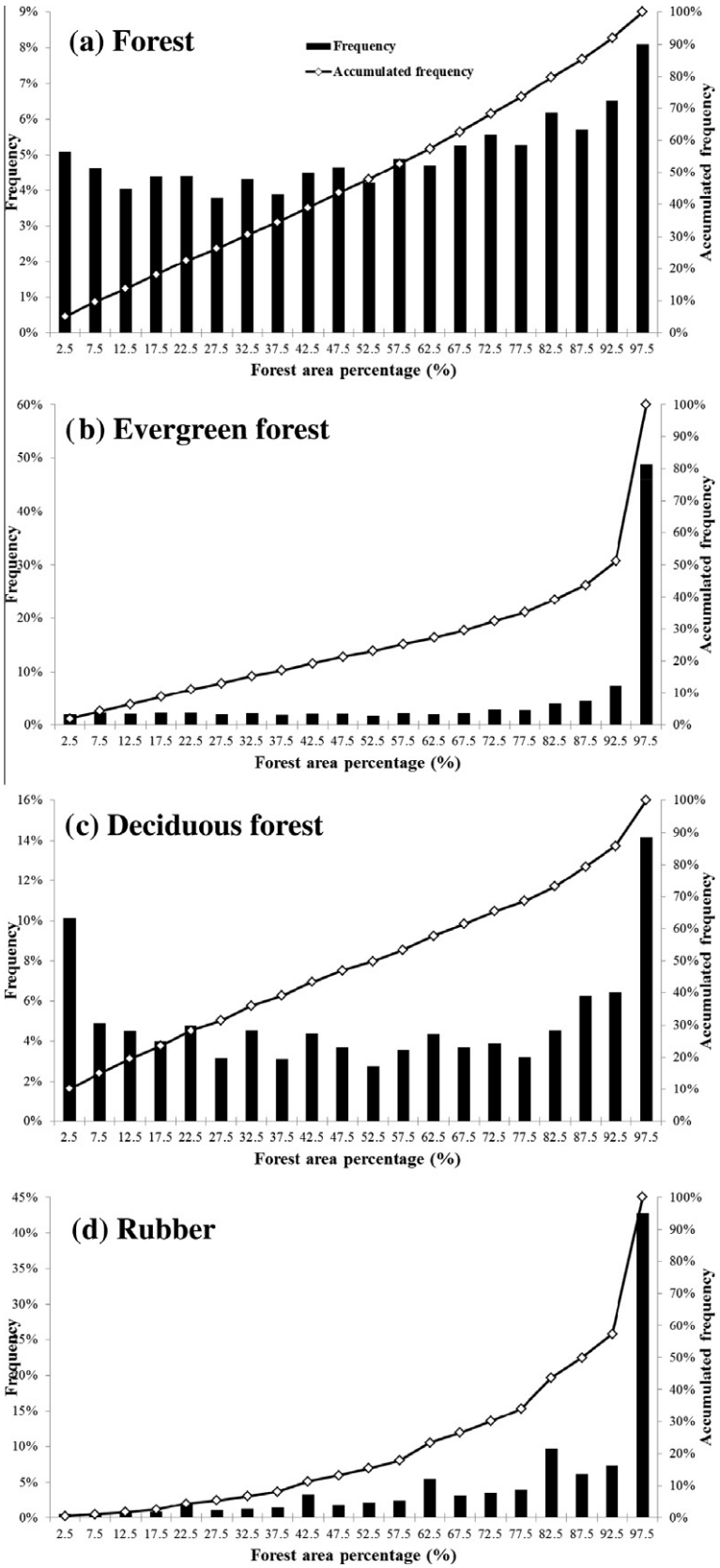

Fig. 7. Frequency histograms of forest area proportion in (a) the entire Hainan Island, (b) evergreen forest pixels, (c) deciduous forest pixels, and (d) rubber plantation pixels.

eral studies have evaluated the potential of PALSAR 50 m mosaic data in forest identification and forest classification (Miettinen and Liew, 2011; Thiel et al., 2009). In this study, we used not only HH and HV polarizations of PALSAR data, but also two new gener-

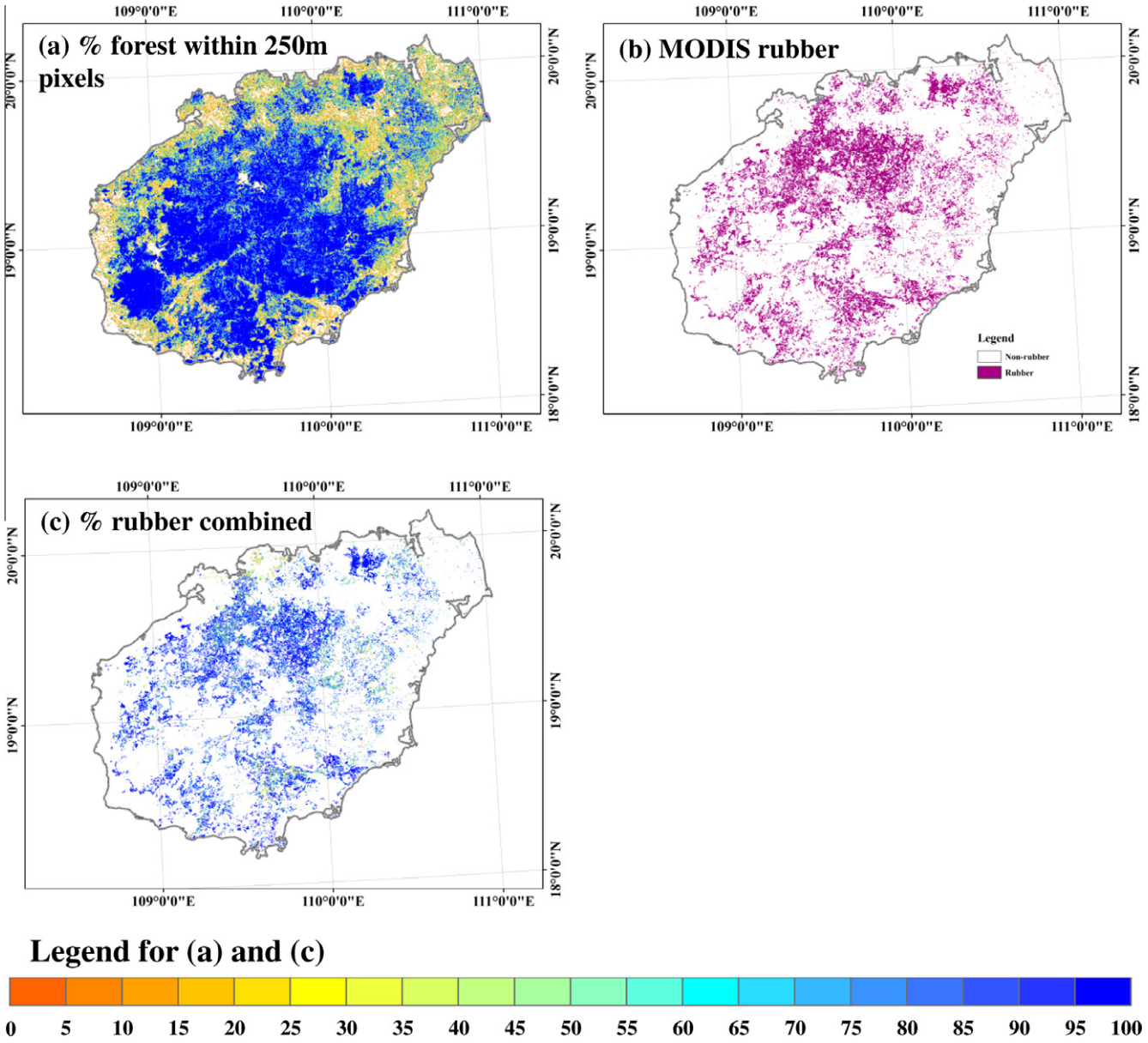

Fig. 8. (a) 250 m forest area percentage map aggregated from the 50 m PALSAR-based forest map; (b) 250 m per-pixel binary map of rubber plantation based on MODIS NDVI data; (c) area percentage map of rubber plantation by combining the forest area percentage map *a* and the 250 m rubber plantation per-pixel binary map *b*.

ated images (Ratio and Difference of HH and HV) that were proved effective. However, more complicated forest type classification methods are less robust than a simple forest/non-forest classification (Walker et al., 2010).

Phenology of forests (deciduous and evergreen forests) in the tropical zone is affected by the seasonality of precipitation (dry season and wet season). Hainan Island has a typical tropical monsoon climate. Deciduous trees lose their leaves to conserve water and avoid transpiration in the dry season (winter) and are so-called tropical seasonal forest in this region. Evergreen trees grow all year but suffer greater water loss during the dry season, and they have different photosynthetic rates and nutrient-use efficiency than deciduous trees (Delucia and Schlesinger, 1995).

The pattern of forest composition (evergreen and deciduous forests) plays an important role in ecological processes and forest carbon cycling. However, due to lack of time series of PALSAR 50 m mosaic data throughout a year, we were not able to map deciduous and evergreen forests from the PALSAR 50 m data. Instead, we used time series MODIS data to generate an evergreen forest map (per-pixel map) and combined that map with the PALSAR-based forest fractional map to estimate evergreen and deciduous forests on Hainan Island. Note that time series imagery from optical sensors (e.g., SPOT-VGT, AVHRR, MODIS) are widely used to generate regional and global maps of evergreen and deciduous forests (DeFries et al., 1995; Liang, 2001; Roderick et al., 1999). The leaf loss of deciduous trees is an important biophysical event to separate evergreen and deciduous forests. Time series data of LSWI were used to separate evergreen and deciduous plants (Xiao et al., 2002), and to map evergreen forests in the pan-tropical zone (Xiao et al., 2009). A comparison between the PALSAR-based forest map and MODIS-based forest map will help evaluate the accuracy of the forest map derived from MODIS imagery. The comparison between the PALSAR-based forest map and the MODIS-based evergreen forest map in the Hainan Island showed that the LSWI-based approach for mapping evergreen forest is robust.

Plantations, or cash forests, are an important land use type and economic activity. Miettinen and Liew (2011) found that the PALSAR 50 m mosaic product can be used to separate rubber, wattles

and palms (oil palm and coconut combined) in known closed canopy plantation areas. PALSAR 50 m mosaic data were used to identify palm plantations in insular Southeast Asia with a method using threshold values (Miettinen et al., 2012). For Hainan Island, two recent studies have used a remote sensing approach to estimate the area of rubber plantations (Zhang et al., 2010; Chen et al., 2010). One study used four Landsat TM images (acquired in May and June 2008) and a supervised classification method to map rubber plantations on the island (Zhang et al., 2010); they estimated a total area of rubber plantations to be 4167.6 km^2, which is about 8% lower than the estimate from the annual official statistical report in 2008. The other study using maximum monthly NDVI composites derived from the MODIS 16-day vegetation indices product (MOD13Q1) estimated a total area of rubber plantation to be 4664 km^2 on Hainan Island in 2009 (Chen et al., 2010).

Together with all the above mentioned studies, our study shows the capabilities of remote sensing methods in forest monitoring and mapping of economically valuable cash plantations. It also highlights the benefits that can be achieved by combining several different types of remotely sensed data. Based on our findings during this study, we believe that the mapping of rubber plantations on Hainan Island could be further improved by combining or fusing the time series of Landsat images and PALSAR 50 m mosaic imagery (Hong et al., 2009).

Finally, we would like to highlight the usability of online photo archives for ground truth purposes. Evaluation (or validation) of land cover maps is a major challenge in the community of remote sensing and land use and land cover change, as it often requires a large number of ground truth data of individual land cover types. In this study, we used ground truth references data from both geo-referenced field photos acquired during field surveys and high-resolution images available in Google Earth. The Global Geo-Referenced Field Photos Library at the University of Oklahoma (http://www.eomf.ou.edu/photos/) allows users to share and archive geo-referenced field photos; those field photos and associated land cover database are downloaded in 'kml' or ESRI shape files online. As of January 2012, there are more than 35,000 high quality geo-referenced field photos in the database, which provides valuable validation references for global land cover classification. In this study we also highlighted the Google Earth based validation workflow. Google Earth's High-Resolution Imagery Archive have high horizontal positional accuracy (Potere, 2008), especially in urban areas, and is convenient for land cover validation in some regions. This method has been used in validation for land cover classification (Benedek and Sziranyi, 2009; Cohen et al., 2010; Gemmell et al., 2009; Montesano et al., 2009). A specific tool that integrates Google Earth with image processing software synchronously could improve the convenience greatly in future.

5. Conclusion

A regional map of tropical forest distributions (e.g. evergreen or deciduous) is imperative for ecological modeling and forest management in pan-tropical regions (Achard et al., 2002). Mapping of the rubber plantation and its spatial distribution is also necessary for not only rubber industry but also regional development and decision making (Li and Fox, 2011). Considering the cloud limitation from traditional optical remote sensing in pan-tropical regions, an integrating approach combining PALSAR 50 m and MODIS imagery was found to be alternative method for mapping forest and rubber plantation in the region, as this method incorporates both cloud-free forest information from PALSAR and phenology information from MODIS. Evergreen and deciduous forests were separated and rubber plantations identified using phenology information based on MODIS temporal profile analysis. We found that the PALSAR 50 m Orthorectified Mosaic Product can be used effectively to delineate forest, cropland, water body and urban land. The sensitivity of rubber plants in Hainan Island to climate makes the rubber separable from other types of forests. This study demonstrated that an integrated strategy combining PALSAR and MODIS data could be more reliable in tropical forest classification and cash forest (e.g. rubber plantation) identification.

Acknowledgements

This study was supported by the NASA Land Use and Land Cover Change Program (NNX09AC39G), the US National Science Foundation (NSF) EPSCoR Program (NSF-0919466), and the Chinese National Key Program for Developing Basic Science (2010CB950900). We thank journal editor Dr. Daniel L. Civco and three reviewers for their valuable suggestions and comments on earlier version of the manuscript.

Appendix A. Supplementary material

Supplementary data associated with this article can be found, in the online version, at http://dx.doi.org/10.1016/j.isprsjprs.2012.07.004. These data include Google maps of the most important areas described in this article.

References

Achard, F., Estreguil, C., 1995. Forest classification of Southeast Asia using NOAA AVHRR data. Remote Sensing of Environment 54 (3), 198–208.
Achard, F., Eva, H., Mayaux, P., 2001. Tropical forest mapping from coarse spatial resolution satellite data: production and accuracy assessment issues. International Journal of Remote Sensing 22 (14), 2741–2762.
Achard, F., Eva, H.D., Stibig, H.J., Mayaux, P., Gallego, J., Richards, T., Malingreau, J.P., 2002. Determination of deforestation rates of the world's humid tropical forests. Science 297 (5583), 999–1002.
Achard, F., DeFries, R., Eva, H., Hansen, M., Mayaux, P., Stibig, H.J., 2007. Pan-tropical monitoring of deforestation. Environmental Research Letters 2 (4), 045022.
Ardila, J.P., Tolpekin, V., Bijker, W., 2010. Angular backscatter variation in L-band ALOS ScanSAR images of tropical forest areas. IEEE Transactions on Geoscience and Remote Sensing 7 (4), 821–825.
Asner, G.P., 2001. Cloud cover in Landsat observations of the Brazilian Amazon. International Journal of Remote Sensing 22 (18), 3855–3862.
Asner, G.P., Knapp, D.E., Broadbent, E.N., Oliveira, P.J.C., Keller, M., Silva, J.N., 2005. Selective logging in the Brazilian Amazon. Science 310 (5747), 480–482.
Baghdadi, N., Boyer, N., Todoroff, P., El Hajj, M., Begue, A., 2009. Potential of SAR sensors TerraSAR-X, ASAR/ENVISAT and PALSAR/ALOS for monitoring sugarcane crops on Reunion Island. Remote Sensing of Environment 113 (8), 1724–1738.
Bartholome, E., Belward, A.S., 2005. GLC2000: a new approach to global land cover mapping from Earth observation data. International Journal of Remote Sensing 26 (9), 1959–1977.
Benedek, C., Sziranyi, T., 2009. Change detection in optical aerial images by a multilayer conditional mixed Markov model. IEEE Transactions on Geoscience and Remote Sensing 47 (10), 3416–3430.
Bond-Lamberty, B., Peckham, S.D., Ahl, D.E., Gower, S.T., 2007. Fire as the dominant driver of central Canadian boreal forest carbon balance. Nature 450 (7166), 89–92.
Cai, Y., 1994. Factor analysis and development strategy of land resource use in Hainan Island. Natural Resources (2), 1–7.
Chen, H., Chen, X., Chen, Z., Zhu, N., Tao, Z., 2010. A primary study on rubber acreage estimation from MODIS-based information in Hainan. Chinese Journal of Tropical Crops 31 (07), 1181–1185.
Christian, H., Narong, C., 2005. Effects of Land Use Changes on Soil Chemical Properties of Sandy Soils from Tropical Hainan, China, Management of Tropical Sandy Soils for Sustainable Agriculture, Khon Kaen, Thailand.
Cohen, W.B., Yang, Z.G., Kennedy, R., 2010. Detecting trends in forest disturbance and recovery using yearly Landsat time series: 2. TimeSync – Tools for calibration and validation. Remote Sensing of Environment 114 (12), 2911–2924.
Collins, M.J., Dymond, C., Johnson, E.A., 2004. Mapping subalpine forest types using networks of nearest neighbour classifiers. International Journal of Remote Sensing 25 (9), 1701–1721.
DeFries, R., Hansen, M., Townshend, J., 1995. Global discrimination of land cover types from metrics derived from AVHRR pathfinder data. Remote Sensing of Environment 54 (3), 209–222.
Delucia, E.H., Schlesinger, W.H., 1995. Photosynthetic rates and nutrient-use efficiency among evergreen and deciduous shrubs in Okefenokee Swamp. International Journal of Plant Sciences 156 (1), 19–28.

Dixon, R.K., Brown, S., Houghton, R.A., Solomon, A.M., Trexler, M.C., Wisniewski, J., 1994. Carbon pools and flux of global forest ecosystems. Science 263 (5144), 185–190.
Foley, J.A., DeFries, R., Asner, G.P., Barford, C., Bonan, G., Carpenter, S.R., Chapin, F.S., Coe, M.T., Daily, G.C., Gibbs, H.K., Helkowski, J.H., Holloway, T., Howard, E.A., Kucharik, C.J., Monfreda, C., Patz, J.A., Prentice, I.C., Ramankutty, N., Snyder, P.K., 2005. Global consequences of land use. Science 309 (5734), 570–574.
Fox, J., Vogler, J.B., 2005. Land-use and land-cover change in montane mainland southeast Asia. Environmental Management 36 (3), 394–403.
Friedl, M.A., McIver, D.K., Hodges, J.C.F., Zhang, X.Y., Muchoney, D., Strahler, A.H., Woodcock, C.E., Gopal, S., Schneider, A., Cooper, A., Baccini, A., Gao, F., Schaaf, C., 2002. Global land cover mapping from MODIS: algorithms and early results. Remote Sensing of Environment 83 (1–2), 287–302.
Gemmell, A.L., Smith, G.C., Haines, K., Blower, J.D., 2009. Validation of ocean model syntheses against hydrography using a new web application. Journal of Operational Oceanography 2 (2), 29–41.
Giri, C., Zhu, Z.L., Reed, B., 2005. A comparative analysis of the Global Land Cover 2000 and MODIS land cover data sets. Remote Sensing of Environment 94 (1), 123–132.
Hong, G., Zhang, Y., Mercer, B., 2009. A wavelet and IHS integration method to fuse high resolution SAR with moderate resolution multispectral images. Photogrammetric Engineering & Remote Sensing 75 (10), 1213–1223.
Huang, C.Q., Goward, S.N., Schleeweis, K., Thomas, N., Masek, J.G., Zhu, Z.L., 2009. Dynamics of national forests assessed using the Landsat record: case studies in eastern United States. Remote Sensing of Environment 113 (7), 1430–1442.
Huang, C., Goward, S.N., Masek, J.G., Thomas, N., Zhu, Z., Vogelmann, J.E., 2010. An automated approach for reconstructing recent forest disturbance history using dense Landsat time series stacks. Remote Sensing of Environment 114 (1), 183–198.
Huete, A.R., Liu, H.Q., Batchily, K., vanLeeuwen, W., 1997. A comparison of vegetation indices over a global set of TM images for EOS-MODIS. Remote Sensing of Environment 59 (3), 440–451.
Huete, A., Didan, K., Miura, T., Rodriguez, E.P., Gao, X., Ferreira, L.G., 2002. Overview of the radiometric and biophysical performance of the MODIS vegetation indices. Remote Sensing of Environment 83 (1–2), 195–213.
Hunan, S.O., 1999. The Past 50 years of Hainan (1949–1999). China Statistics Press.
Kabir, S., He, D.C., Sanusi, M.A., Hussin, W.M.A.W., 2010. Texture analysis of IKONOS satellite imagery for urban land use and land cover classification. Imaging Science Journal 58 (3), 163–170.
Kavzoglu, T., 2009. Increasing the accuracy of neural network classification using refined training data. Environmental Modelling & Software 24 (7), 850–858.
Kummer, D.M., Turner, B.L., 1994. The human causes of deforestation in Southeast-Asia. Bioscience 44 (5), 323–328.
Lelieveld, J., Butler, T.M., Crowley, J.N., Dillon, T.J., Fischer, H., Ganzeveld, L., Harder, H., Lawrence, M.G., Martinez, M., Taraborrelli, D., Williams, J., 2008. Atmospheric oxidation capacity sustained by a tropical forest. Nature 452 (7188), 737–740.
Li, Z., Fox, J.M., 2011. Integrating Mahalanobis typicalities with a neural network for rubber distribution mapping. Remote Sensing Letters 2 (2), 157–166.
Li, Z., Fox, J.M., 2012. Mapping rubber tree growth in mainland Southeast Asia using time-series MODIS 250 m NDVI and statistical data. Applied Geography 32 (2), 420–432.
Li, H.M., Aide, T.M., Ma, Y.X., Liu, W.J., Cao, M., 2007. Demand for rubber is causing the loss of high diversity rain forest in SW China. Biodiversity and Conservation 16 (6), 1731–1745.
Liang, S., 2001. Land-cover classification methods for multi-year AVHRR data. International Journal of Remote Sensing 22 (8), 1479–1493.
Lin, M., Zhang, Y., 2001. Dynamic change of tropical forest in Hainan Island. Geographical Research 20 (06), 703–712.
Liu, J.Y., Deng, X.Z., 2010. Progress of the research methodologies on the temporal and spatial process of LUCC. Chinese Science Bulletin 55 (14), 1354–1362.
Liu, J.Y., Liu, M.L., Tian, H.Q., Zhuang, D.F., Zhang, Z.X., Zhang, W., Tang, X.M., Deng, X.Z., 2005. Spatial and temporal patterns of China's cropland during 1990–2000: an analysis based on Landsat TM data. Remote Sensing of Environment 98 (4), 442–456.
Liu, J.Y., Zhang, Z.X., Xu, X.L., Kuang, W.H., Zhou, W.C., Zhang, S.W., Li, R.D., Yan, C.Z., Yu, D.S., Wu, S.X., Nan, J., 2010. Spatial patterns and driving forces of land use change in China during the early 21st century. Journal of Geographical Sciences 20 (4), 483–494.
Longepe, N., Rakwatin, P., Isoguchi, O., Shimada, M., Uryu, Y., Yulianto, K., 2011. Assessment of ALOS PALSAR 50 m orthorectified FBD data for regional land cover classification by support vector machines. IEEE Transactions on Geoscience and Remote Sensing 49 (6), 2135–2150.
Luckman, A., Baker, J., Honzak, M., Lucas, R., 1998. Tropical forest biomass density estimation using JERS-1 SAR: seasonal variation, confidence limits, and application to image mosaics. Remote Sensing of Environment 63 (2), 126–139.
Miettinen, J., Liew, S.C., 2011. Separability of insular Southeast Asian woody plantation species in the 50 m resolution ALOS PALSAR mosaic product. Remote Sensing Letters 2 (4), 299–307.
Miettinen, J., Shi, C., Tan, W.J., Chinliew, S., 2012. 2010 land cover map of insular Southeast Asia in 250-m spatial resolution. Remote Sensing Letters 3 (1), 11–20.
Montesano, P.M., Nelson, R., Sun, G., Margolis, H., Kerber, A., Ranson, K.J., 2009. MODIS tree cover validation for the circumpolar taiga–tundra transition zone. Remote Sensing of Environment 113 (10), 2130–2141.
Morton, D.C., DeFries, R.S., Shimabukuro, Y.E., Anderson, L.O., Espirito-Santo, F.D.B., Hansen, M., Carroll, M., 2005. Rapid assessment of annual deforestation in the Brazilian Amazon using MODIS data. Earth Interactions 9 (8), 1–22.
Page, S.E., Siegert, F., Rieley, J.O., Boehm, H.D.V., Jaya, A., Limin, S., 2002. The amount of carbon released from peat and forest fires in Indonesia during 1997. Nature 420 (6911), 61–65.
Perea, A.J., Merono, J.E., Aguilera, M.J., de la Cruz, J.L., 2010. Land-cover classification with an expert classification algorithm using digital aerial photographs. South African Journal of Science 106 (5–6), 82–87.
Pielke, R.A., 2005. Land use and climate change. Science 310 (5754), 1625–1626.
Potere, D., 2008. Horizontal positional accuracy of Google earth's high-resolution imagery archive. Sensors 8 (12), 7973–7981.
Qiu, J., 2009. Where the rubber meets the garden. Nature 457 (7227), 246–247.
Ranson, K.J., Sun, G.Q., 1994. Northern forest classification using temporal multifrequency and multipolarimetric Sar images. Remote Sensing of Environment 47 (2), 142–153.
Richards, J.A., Jia, X., 2006. Remote Sensing Digital Image Analysis: An Introduction, fourth ed. Springer, Berlin.
Roderick, M.L., Noble, I.R., Cridland, S.W., 1999. Estimating woody and herbaceous vegetation cover from time series satellite observations. Global Ecology and Biogeography 8 (6), 501–508.
Rosenqvist, A., Shimada, M., Ito, N., Watanabe, M., 2007. ALOS PALSAR: a pathfinder mission for global-scale monitoring of the environment. IEEE Transactions on Geoscience and Remote Sensing 45 (11), 3307–3316.
Sakaguchi, K., Zeng, X.B., Christoffersen, B.J., Restrepo-Coupe, N., Saleska, S.R., Brando, P.M., 2011. Natural and drought scenarios in an east central Amazon forest: fidelity of the Community Land Model 3.5 with three biogeochemical models. Journal of Geophysical Research 116, G01029.
Santoro, M., Fransson, J.E.S., Eriksson, L.E.B., Ulander, L.M.H., 2010. Clear-cut detection in Swedish boreal forest using multi-temporal ALOS PALSAR backscatter data. IEEE Journal of Selected Topics in Applied Earth Observations and Remote Sensing 3 (4), 618–631.
Simard, M., Saatchi, S.S., De Grandi, G., 2000. The use of decision tree and multiscale texture for classification of JERS-1 SAR data over tropical forest. IEEE Transactions on Geoscience and Remote Sensing 38 (5), 2310–2321.
Simard, M., De Grandi, G., Saatchi, S., Mayaux, P., 2002. Mapping tropical coastal vegetation using JERS-1 and ERS-1 radar data with a decision tree classifier. International Journal of Remote Sensing 23 (7), 1461–1474.
Stibig, H.J., Malingreau, J.P., 2003. Forest cover of insular southeast Asia mapped from recent satellite images of coarse spatial resolution. Ambio 32 (7), 469–475.
Stibig, H.J., Achard, F., Fritz, S., 2004. A new forest cover map of continental southeast Asia derived from SPOT-VEGETATION satellite imagery. Applied Vegetation Science 7 (2), 153–162.
Su, W., Zhang, C., Yang, J.Y., Wu, H.G., Chen, M.J., Yue, A.Z., Zhang, Y.N., Sun, C., 2010. Knowledge-based object oriented land cover classification using SPOT5 imagery in forest-agriculture ecotones. Sensor Letters 8 (1), 22–31.
Thessler, S., Sesnie, S., Bendana, Z.S.R., Ruokolainen, K., Tomppo, E., Finegan, B., 2008. Using k-nn and discriminant analyses to classify rain forest types in a Landsat TM image over northern Costa Rica. Remote Sensing of Environment 112 (5), 2485–2494.
Thiel, C.J., Thiel, C., Schmullius, C.C., 2009. Operational large-area forest monitoring in Siberia using ALOS PALSAR summer intensities and winter coherence. IEEE Transactions on Geoscience and Remote Sensing 47 (12), 3993–4000.
Torbick, N., Salas, W.A., Hagen, S., Xiao, X.M., 2011. Monitoring rice agriculture in the Sacramento Valley, USA with multitemporal PALSAR and MODIS imagery. IEEE Journal of Selected Topics in Applied Earth Observations and Remote Sensing 4 (2), 451–457.
Tottrup, C., Rasmussen, M.S., Eklundh, L., Jonsson, P., 2007. Mapping fractional forest cover across the highlands of mainland Southeast Asia using MODIS data and regression tree modelling. International Journal of Remote Sensing 28 (1–2), 23–46.
Townsend, P.A., 2002. Estimating forest structure in wetlands using multitemporal SAR. Remote Sensing of Environment 79 (2–3), 288–304.
Townshend, J.R.G., Justice, C.O., 1988. Selecting the spatial-resolution of satellite sensors required for global monitoring of land transformations. International Journal of Remote Sensing 9 (2), 187–236.
Tucker, C.J., 1979. Red and photographic infrared linear combinations for monitoring vegetation. Remote Sensing of Environment 8 (2), 127–150.
Walker, W.S., Stickler, C.M., Kellndorfer, J.M., Kirsch, K.M., Nepstad, D.C., 2010. Large-area classification and mapping of forest and land cover in the Brazilian Amazon: a comparative analysis of ALOS/PALSAR and Landsat data sources. IEEE Journal of Selected Topics in Applied Earth Observations and Remote Sensing 3 (4), 594–604.
Wu, F., Wang, C., Zhang, H., Zhang, B., Tang, Y.X., 2011. Rice crop monitoring in South China with RADARSAT-2 quad-polarization SAR data. IEEE Transactions on Geoscience and Remote Sensing 8 (2), 196–200.
Xiao, X.M., Boles, S., Liu, J.Y., Zhuang, D.F., Liu, M.L., 2002. Characterization of forest types in Northeastern China, using multi-temporal SPOT-4 VEGETATION sensor data. Remote Sensing of Environment 82 (2–3), 335–348.
Xiao, X.M., Hollinger, D., Aber, J., Goltz, M., Davidson, E.A., Zhang, Q.Y., Moore, B., 2004. Satellite-based modeling of gross primary production in an evergreen needleleaf forest. Remote Sensing of Environment 89 (4), 519–534.
Xiao, X.M., Zhang, Q.Y., Hollinger, D., Aber, J., Moore, B., 2005. Modeling gross primary production of an evergreen needleleaf forest using modis and climate data. Ecological Applications 15 (3), 954–969.

Xiao, X., Biradar, C., Czarnecki, C., Alabi, T., Keller, M., 2009. A simple algorithm for large-scale mapping of evergreen forests in tropical America, Africa and Asia. Remote Sensing 1 (3), 355–374.

Xiao, W., Wang, X., Ling, F., 2010. The application of ALOS PALSAR data on mangrove forest extraction. Remote Sensing Technology and Application 25 (01), 91–96.

Xie, C., Li, Z., Li, X., 2010. A study of deformation in permafrost regions of Qinghai-Tibet Plateau based on ALOS/PALSAR D-InSAR interferometry. Remote Sensing for Land & Resources 30 (01), 53–56.

Xu, X.L., Zeng, L., Zhuang, D.F., 2002. Analysis on land-use change and socio-economic driving factors in Hainan Island during 50 years from 1950 to 1999. Chinese Geographical Science 12 (3), 193–198.

Yang, Y., Li, Z., Chen, e., Ling, F., 2010. Recognition of forest cover based on multi-temporal dual polarization ALOS PALSAR data. Journal of Anhui Agricultural Sciences 38 (18), 9840–9844.

Zhang, J., Tao, Z., Liu, S., Cai, D., Tian, G., Xie, R., Xu, X., 2010. Rubber planting acreage calculation in Hainan Island based on TM image. Chinese Journal of Tropical Crops 31 (04), 661–665.

Ziegler, A.D., Fox, J.M., Xu, J.C., 2009. The rubber juggernaut. Science 324 (5930), 1024–1025.